Quasielastic and low vibrational lineshapes in atom–surface diffusion

2004 J. Phys.: Condens. Matter 16 S2879

(http://iopscience.iop.org/0953-8984/16/29/003)

INSTITUTE OF PHYSICS PUBLISHING JOURNAL OF PHYSICS: CONDENSED MATTER

J. Phys.: Condens. Matter **16** (2004) S2879–S2894 PII: S0953-8984(04)80315-1

Quasielastic and low vibrational lineshapes in atom–surface diffusion

J L Vega, R Guantes and S Miret-Artés

Instituto de Matemáticas y Física Fundamental, Consejo Superior de Investigaciones Científicas, Serrano 123, 28006 Madrid, Spain

E-mail: jlvega@imaff.cfmac.csic.es, rgn@imaff.cfmac.csic.es and s.miret@imaff.cfmac.csic.es

Received 4 May 2004
Published 9 July 2004
Online at stacks.iop.org/JPhysCM/16/S2879
doi:10.1088/0953-8984/16/29/003

Abstract

The diffusion and low frequency vibrational motions of atoms and molecules on surfaces can be measured by means of quasielastic helium atom scattering. In this paper, we discuss and investigate different analytical approximations, based on the theory of stochastic processes, to the dynamic structure factor, considering the two motions on an equal footing. Special emphasis is put on the nature of the corresponding lineshapes, explained in terms of the motional narrowing effect. We also discuss the influence of the diffusional and vibrational coupling and several ways of experimentally separating the two types of contributions to the dynamic structure factor. In particular, we propose that the so-called inelastic focusing singularity from atom–surface scattering controls the lineshapes of quasielastic and vibrational peaks.

1. Introduction

Diffusional and vibrational motions of adsorbates on surfaces are two elementary dynamical processes which are of paramount importance in surface physics. The quasielastic helium atom scattering (QHAS) technique has revealed itself as an alternative and very convenient tool for analysing both diffusion [1–5] and low frequency vibrations [6–9] of adsorbates on surfaces. From time-of-flight measurements, converted to an energy transfer scale, a wide energy range can be spanned and several peaks are easily observed. First, a prominent peak around zero energy transfer, known as the quasielastic peak (Q-peak), gives us information about the diffusion motion. Second, some peaks, due to energy exchange with surface phonons such as the Rayleigh wave (RW) and the longitudinal resonance (LR), provide information about inelastic scattering with the surface. And third, additional weaker peaks at low energy transfers

(creation and annihilation processes) are attributed to frustrated translations of adsorbates parallel to the surface (T-modes). Theoretically, the corresponding lineshapes of the Q- and T-peaks are given by the dynamic structure factor $S(\mathbf{K}, \omega)$, which is defined as the space–time Fourier transform of the van Hove distribution function $G(\mathbf{R}, t)$ [10, 11]. At low adatom concentrations, interactions between adsorbates can be ignored, and $G(\mathbf{R}, t)$ gives the probability of finding a single adatom at the lattice position $\mathbf{R}$ at time t, given that it was at the origin at some arbitrary time $t = 0$.

In order to extract useful information about the adsorbate dynamics (diffusion mechanisms and coefficients, jump distributions or vibrational frequencies) as well as details of the adsorbate–surface interaction (diffusion barriers, friction constants or adiabatic atom–surface potentials), some approximate theory is needed relating the dynamic structure factor to relevant physical parameters. Traditionally two simple models have been used to obtain information about the diffusional dynamics: at small wavevector transfers (probing large distances) the potential structure plays almost no role and the adsorbate is modelled as a particle subject to thermal noise and dissipation; that is, as a Gaussian stochastic process whose probability density is the solution of the standard diffusion equation. From this model the diffusion coefficient can be inferred, as briefly explained below. In contrast, at larger wavevector transfers, the potential structure plays an important role and it is usually taken into account by assuming discrete instantaneous jumps between different sites on the surface (the Chudley–Elliot model [12]). Within this model, jump distributions can be easily calculated. In both cases, the Q-peak lineshape is a Lorentzian profile. On the other hand, the T-mode peak, with the surface temperature, shows an approximately linear shift and broadening which have been explained assuming transitions from a Boltzmann population of vibrational levels of an anharmonic oscillator [6]. This provides information about the curvature of the adiabatic interaction potential and the friction coefficient when extrapolated to zero temperature. Again, the lineshape of the peak has been assumed to be Lorentzian. In any case, a detailed analysis of the different lineshapes for the Q- and T-peaks is still lacking in the literature.

Diffusion and low frequency vibration motions are governed by different length scales and timescales and this is why most of the time they are treated separately. However, it is known that they become coupled when the scaled surface temperature kT is similar to or higher than the diffusion barrier height and the wavevector transfer of the probe particles is large [13, 14]. As far as we know, the first attempt to consider the two kinds of motions on equal footing is due to Chen and Ying [13] who used a microscopic theory based on Mori's projection operator formalism [15]. Alternative stochastic theories within the Fokker–Planck formalism [16] or the equivalent Langevin formalism [17, 18] have been successfully applied to interpret QHAS experiments classically [2, 3, 8, 13, 14, 19, 20] or quantum mechanically [21]. Both motions are therefore considered as stochastic processes although their dynamics are determined by different parts of the interaction potential.

In this paper we discuss in some detail the relevant physical parameters governing the adsorbate dynamics (both diffusional and vibrational) and how they can be related to observable features such as lineshapes and different sources of broadening by using simple stochastic theories. In particular, we will show that the corresponding lineshapes are governed by the motional narrowing [22] effect first observed in the stochastic nuclear magnetic resonance lineshapes [23]. Moreover, we also propose an experimental way to separate the two kinds of motion by means of an adequate manipulation of the initial conditions of the atomic beam. This is the so-called focusing effect and its implication in diffusion and vibrational low frequency mode spectroscopy has not been investigated yet. Focusing processes have been extensively exploited in continuum state surface scattering [24], elastic and inelastic selective adsorption resonances [25] and sticking problems [26].

2. Diffusion lineshapes

It is convenient to express the dynamic structure factor directly in terms of the intermediate scattering function $I(\mathbf{K}, t)$ [27], the space Fourier transform of the van Hove correlation function, as

$$S(\mathbf{K}, \omega) = \int_{-\infty}^{\infty} \mathrm{e}^{-\mathrm{i}\omega t} I(\mathbf{K}, t)\, \mathrm{d}t. \tag{1}$$

The function $I(\mathbf{K}, t)$ can be considered as the characteristic function of the stochastic process $\mathbf{R}(t)$:

$$I(\mathbf{K}, t) = \langle \mathrm{e}^{-\mathrm{i}\mathbf{K}[\mathbf{R}(t)-\mathbf{R}(0)]} \rangle = \langle \mathrm{e}^{-\mathrm{i}\mathbf{K}\int_0^t v_{\mathbf{K}}(t')\,\mathrm{d}t'} \rangle \tag{2}$$

where $v_{\mathbf{K}}$ is the velocity of the adparticle projected along the wavevector transfer $\mathbf{K}$ direction.

A cumulant expansion to second order yields the standard result [28]

$$I(\mathbf{K}, t) \sim \mathrm{e}^{-\frac{\mathbf{K}^2}{2}\int_0^t \mathrm{d}t' \int_0^t \mathrm{d}t'' \langle v_{\mathbf{K}}(t') v_{\mathbf{K}}(t'') \rangle} = \mathrm{e}^{-\mathbf{K}^2 \int_0^t (t-t')\psi(t')\,\mathrm{d}t'} \tag{3}$$

where $\psi(t) \equiv \langle v_{\mathbf{K}}(t) v_{\mathbf{K}}(0) \rangle$ is the velocity autocorrelation function. The first approximation comes from the truncation of the cumulant series, and the second equality holds if the velocity process $v_{\mathbf{K}}(t)$ is stationary. For Gaussian stochastic processes, as when the thermal noise is Gaussian white noise and there is no interaction potential or it is quadratic, equation (3) is exact.

If a stochastic process is Gaussian and Markovian, Doob's theorem states that its correlation function decays in time exponentially. If we assume simply

$$\psi(t) = \langle v_{\mathbf{K}}^2 \rangle \mathrm{e}^{-t/\tau_{\mathrm{c}}} \tag{4}$$

with τ_{c} the (normalized) correlation time for the adparticle velocity,

$$\tau_{\mathrm{c}} \equiv \frac{1}{\langle v_{\mathbf{K}}^2 \rangle} \int_0^{\infty} \langle v_{\mathbf{K}}(t) v_{\mathbf{K}}(0) \rangle\, \mathrm{d}t, \tag{5}$$

the intermediate scattering function can be expressed now as [28]

$$I(\mathbf{K}, t) = \exp\left[-\chi^2 \left(\mathrm{e}^{-t/\tau_{\mathrm{c}}} + \frac{t}{\tau_{\mathrm{c}}} - 1 \right) \right] \tag{6}$$

with

$$\chi = \tau_{\mathrm{c}} \sqrt{\langle v_{\mathbf{K}}^2 \rangle} |\mathbf{K}| = \frac{D|\mathbf{K}|}{\sqrt{\langle v_{\mathbf{K}}^2 \rangle}} \equiv \bar{l}|\mathbf{K}| \tag{7}$$

where $\bar{l}$ is the mean free path and

$$D = \tau_{\mathrm{c}} \langle v_{\mathbf{K}}^2 \rangle \tag{8}$$

is the diffusion coefficient. Note that, for a particle with no adiabatic interaction potential and under thermal noise and dissipation, $\tau_{\mathrm{c}} = 1/\gamma$ [29] where γ is the friction coefficient. In general, equation (8) combined with (5) is the Green–Kubo relation for the diffusion coefficient and therefore, under the Gaussian approximation, the intermediate scattering function contains the exact diffusion coefficient through the parameter χ. This parameter will govern the dynamical coherence of the diffusion process and thus the lineshape of the Q-peak. In the limit $\chi \to \infty$ or, equivalently, $\tau_{\mathrm{c}} \to \infty$ or $\bar{l} \to \infty$, we obtain a Gaussian function (short time approximation, $t \ll \tau_{\mathrm{c}}$)

$$I(\mathbf{K}, t) \propto \mathrm{e}^{-D|\mathbf{K}|^2 t^2/2\tau_{\mathrm{c}}} \tag{9}$$

and the corresponding dynamic structure factor has a Gaussian shape

$$S(\mathbf{K},\omega) \propto \frac{1}{|\mathbf{K}|v_0}\exp[-\omega^2/2|\mathbf{K}|^2v_0^2] \tag{10}$$

with the isotropic mean velocity $v_0 = \sqrt{\langle v_{\mathbf{K}}^2\rangle} = \sqrt{D/\tau_c}$. The corresponding full width at half-maximum (FWHM) is linearly dependent on the wavevector transfer and v_0, $\Gamma \propto v_0|\mathbf{K}|$. The physical meaning of this result is clear. The corresponding van Hove function is of the form

$$G(\mathbf{R},t) \propto \frac{1}{(v_0t)^2}\exp[-\mathbf{R}^2/(t^2v_0^2)] \tag{11}$$

which is interpreted as the probability for the particle to be displaced by $\mathbf{R}$ in a time t assuming a constant velocity $\mathbf{R}/t$ and an initial Maxwell–Boltzmann distribution of velocities, with $v_0 = \sqrt{k_BT/m}$ (two degrees of freedom). This means that for times much shorter than the mean collision time the particle behaves as almost free and dynamical coherence dominates, that is, particles keep a memory of their velocity and variations of probability take place over distances smaller than the mean free path. This behaviour has been found in QHAS experiments of Xe adsorbates on a Pt(111) surface [30], providing evidence for a fully mobile two-dimensional gas of Xe atoms.

In the opposite case, $\chi \ll 1$, we have the long time approximation ($t \gg \tau_c$ in equation (6)),

$$I(\mathbf{K},t) \propto \mathrm{e}^{-\mathbf{K}^2Dt}, \tag{12}$$

and the spectrum has the Lorentzian shape

$$S(\mathbf{K},\omega) \propto \frac{|\mathbf{K}|^2D}{\omega^2+|\mathbf{K}|^4D^2}. \tag{13}$$

Here correlations between different velocities are completely lost and the process is purely diffusive. The FWHM is $\Gamma = 2D\mathbf{K}^2$.

The exact Fourier transform of equation (6) for all ranges of time can be expressed in terms of the complete and incomplete gamma functions as

$$\begin{aligned} S(\mathbf{K},\omega) &= \frac{\mathrm{e}^{\chi^2}\tau_c}{\pi}\chi^{-2\chi^2}\,\mathrm{Re}\,\chi^{-\mathrm{i}2\omega\tau_c}[\Gamma(\chi^2+\mathrm{i}\omega\tau_c)-\Gamma(\chi^2+\mathrm{i}\omega\tau_c,\chi^2)] \\ &= \frac{\mathrm{e}^{\chi^2}}{2\pi}\sum_{n=0}^{\infty}\frac{(-1)^n\chi^{2n}}{n!}\frac{2[(\chi^2+n)/\tau_c]}{\omega^2+[(\chi^2+n)/\tau_c]^2}. \end{aligned} \tag{14}$$

As the value of the parameter χ decreases, the dynamic structure factor goes from a nearly Gaussian to a Lorentzian lineshape and the spectrum becomes narrower and narrower. This general effect is called *motional narrowing* [22]. Not only can the spectrum as a whole be approximated by one of those shapes depending on the value of χ, but, by the general property of the Fourier transform, we see that around $\omega = 0$ the behaviour of $S(\mathbf{K},\omega)$ is governed by the behaviour of the intermediate scattering function at large t and, for large ω, by the corresponding behaviour at small t. Therefore, the shape of the quasielastic peak at the centre will be close to Lorentzian while the wings are close to a Gaussian form. Moreover, from the second expression in equation (14), it is clearly seen that an infinite number of Lorentzian shapes are contributing to the Q-peak, each of them with a width proportional to the diffusion coefficient D plus a contribution increasing linearly with n. Obviously, equation (13) is obtained from equation (14) if only the first term of the series is considered.

This motional narrowing effect is illustrated in figure 1. Here we plot the dynamic structure factor for a particle with no adiabatic interaction potential (white circles) and the theoretical

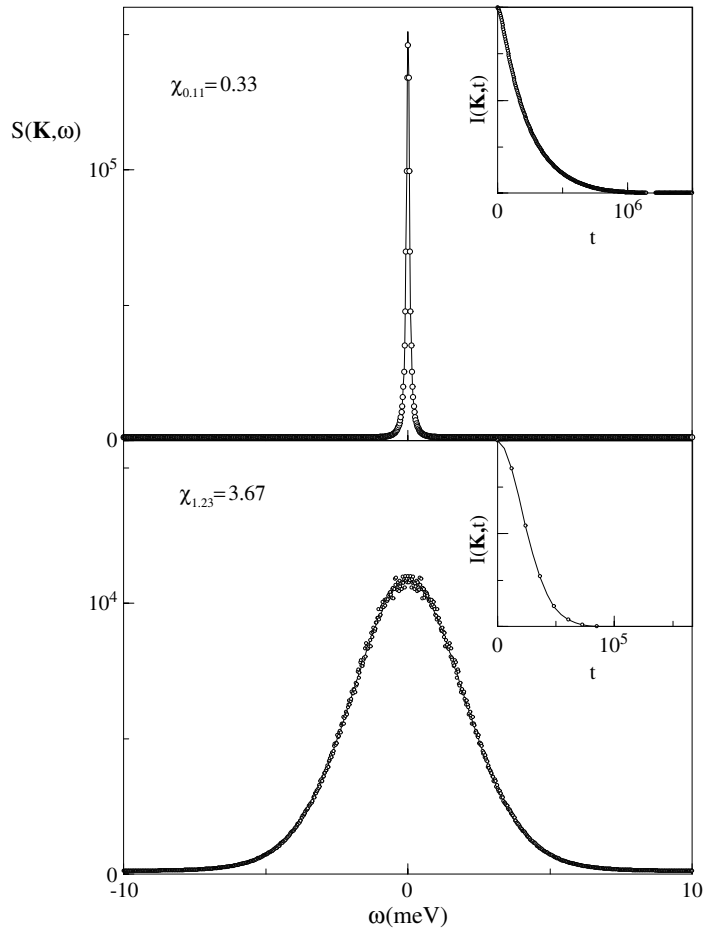

Figure 1. Numerical (white circles) and theoretical (equation (14); solid curves) dynamic structure factors when no interaction potential is considered, at $T = 200$ K and different wavevector transfers: upper panel, $\mathbf{K} = 0.11$ Å^{-1}; lower panel, $\mathbf{K} = 1.23$ Å^{-1}. The values of $\chi = 0.33$ and 3.67 show a Lorentzian and Gaussian lineshape, respectively. In the insets, the corresponding intermediate scattering functions are also plotted.

prediction (solid curves, given by equation (14)) at $T = 200$ K and two different $\mathbf{K}$ values, 0.11 and 1.23 Å^{-1}. The parameter χ defined by equation (7) takes the values 0.33 and 3.67, respectively, showing a clear transition between a Lorentzian and a Gaussian profile. Notice also that the FWHM of the Q-peak is almost one order of magnitude smaller in the Lorentzian case. In the insets, the corresponding intermediate scattering functions are also plotted.

An important point is determining the range of $\mathbf{K}$ values for which the Gaussian approximation, equation (3), is valid for the intermediate scattering function in a realistic surface diffusion system. It is well known that at large wavevector transfers the behaviour of the FWHM is not quadratic in $\mathbf{K}$ as in equation (13), since the structure of the surface has to be taken into account and the Gaussian approximation fails. The simplest model including the periodicity of the surface is due to Chudley and Elliot [12] who proposed a master equation for the van Hove function assuming instantaneous discrete jumps on a two-dimensional Bravais

lattice. This gives again an exponential for the intermediate scattering function

$$I(\mathbf{K}, t) = I(\mathbf{K}, 0)\mathrm{e}^{-t/\tau_1(\mathbf{K})} \tag{15}$$

where the correlation time $\tau_1(\mathbf{K})$ has a periodic dependence in $\mathbf{K}$ of the form

$$\tau_1^{-1}(\mathbf{K}) = \nu \sum_{\mathbf{j}} P_{\mathbf{j}}[1 - \cos(\mathbf{j} \cdot \mathbf{K})], \tag{16}$$

ν being the total rate of jumps out of an adsorption site and $P_{\mathbf{j}}$ the relative probability for a jump with a displacement vector $\mathbf{j}$. For small $\mathbf{K}$ values, and considering uncorrelated jumps in the parallel directions, we see that

$$\tau_1^{-1}(K_{x,y}) \sim \frac{\nu}{2} \sum_j P_j j^2 K_{x,y}^2 = \frac{\nu}{2} \langle j^2 \rangle K_{x,y}^2 \tag{17}$$

where P_j is now the probability of jumping over j lattice sites in a single jump along the x or y direction and $K_{x,y}$ is the wavevector transfer in this direction. From the expression for the diffusion coefficient within the jump diffusion model [31],

$$D = \frac{\nu}{2} \langle j^2 \rangle, \tag{18}$$

we recover the Lorentzian approximation in the long time limit, equation (13).

In order to illustrate the preceding discussion, we choose a prototype model for atom–surface diffusion: Na adatoms at low coverages on a symmetric Cu(100) surface. This model has been investigated exhaustively both experimentally [1–4] and theoretically [1, 3, 13, 14, 19] using different approaches. From numerical simulations and extensive fitting to experiments, an accurate two-dimensional potential energy surface (PES) has been proposed in [2, 3]. The important PES parameters for our discussion of this system are the barrier height for diffusion, $V^{\ddagger} = 75$ meV along x or y directions, and the T-mode peak position extrapolated to zero temperature, $\omega_0 = 6$ meV (which is consistent with the theoretical value of the well frequency $\omega_0 = 2\pi\sqrt{V^{\ddagger}/2ma^2}$, where m is the particle mass and a the unit cell length). The friction coefficient has been also estimated from extrapolation of the T-peak width and comparison between experiment and Langevin simulations, giving $\gamma = 0.1\omega_0$. We take this PES and these parameter values as our starting point for numerical simulations, solving the Langevin equation

$$\ddot{\mathbf{R}} = -\frac{\nabla V(\mathbf{R})}{m} - \gamma \dot{\mathbf{R}} + F_{\mathbf{r}}(t) \tag{19}$$

by a third-order velocity Verlet algorithm [32].

The relevant correlation functions are determined by averaging over appropriate ensembles of trajectories. As a first comparison, in figure 2 we show the FWHM predicted by equation (13) versus the width obtained by a Lorentzian fit of the numerical dynamic structure factor at $T = 150$ K. First, we note that for the whole temperature range spanned experimentally ($50 < T < 350$ K) the values of the parameter χ in equation (7) are such that the Lorentzian shape remains a very good approximation. Secondly, only for $\mathbf{K} < 0.15$ Å^{-1} is the Gaussian approximation accurate for diffusion. The Chudley–Elliot model, however, gives a good fit of the FWHM of the Q-peak as a function of $\mathbf{K}$ for the whole region except at values close to the first Brillouin zone border, where diffusion and vibration start overlapping significantly [14].

Note that equation (16) is in fact a cosine Fourier series, so that using the inversion formula for the Fourier coefficients, the total jump rate and jump distributions along specific parallel directions can be obtained from the FWHM, assuming a Lorentzian shape for the Q-peak. In practice one has two sources of error in this procedure: first, the instantaneous jump picture is a good approximation only for barriers $V^{\ddagger}/kT \geqslant 3$ [16, 14]; second, and more

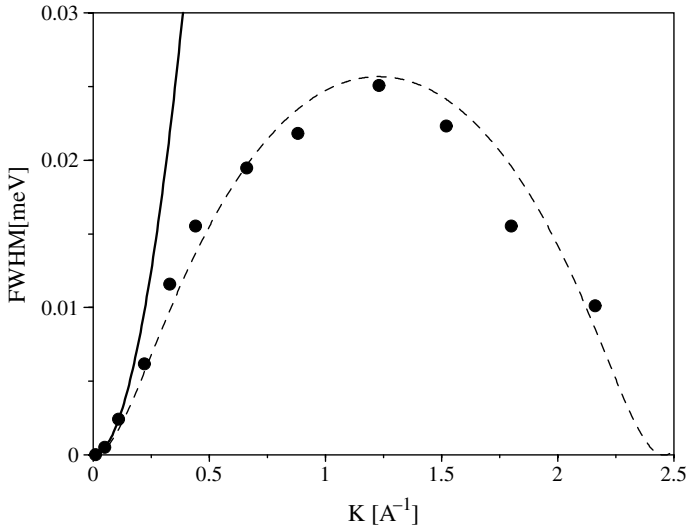

Figure 2. The full width at half-maximum (FWHM) of the Q-peak at $T = 150$ K as a function of the wavevector transfer for the Na/Cu(110) system (see the text). Full circles: Lorentzian fitting to a numerical Langevin simulation. The prediction of the Chudley–Elliot model, equations (15) and (16), is plotted with a dashed line. Solid curve: the FWHM of the Gaussian approximation, equation (13), with the numerically calculated diffusion coefficient.

importantly, the FWHM is not really a periodic function of **K** whose period is a reciprocal lattice vector [1, 3]. This is due to the fact that at large values of the wavevector transfer the contribution of the vibrational T-mode to the quasielastic peak width is appreciable, and diffusional and vibrational motions cannot be separated. Recently, we have shown [14] that in fact jump rates and distributions can be calculated analytically to a very good approximation (again, for barriers $V^{\ddagger}/kT \geqslant 3$) by using Kramers' turnover theory generalized to periodic potentials [33]. Kramers' approach has the advantage that the FWHM within the Chudley–Elliot model can be estimated using only two physical parameters: an effective jump frequency and the energy loss of the particle to the bath as it traverses from one barrier to the next. These two parameters will determine the whole diffusion process if diffusion is activated and not strongly coupled to vibration. Moreover, these two parameters are easily related to the curvature of the potential energy at the barrier and the friction coefficient, and therefore one can easily estimate barrier heights and friction constants from a fitting to the experiment by means of the generalized Kramers' model [14].

3. Low vibration lineshapes

The Gaussian approximation to the intermediate scattering function, equation (3), can also be the starting point for an analytical investigation of the T-mode peak. Now, the important adsorbate dynamics takes place close to the bottom of the potential well and this can be expanded in a Taylor series in **R**. Retaining only the first term we have a parabolic potential and equation (3) is exact. The velocity autocorrelation function for the harmonic oscillator has the form [34]

$$\psi(t) = \langle v_{\mathbf{K}}^2 \rangle \mathrm{e}^{-\frac{\gamma}{2}t} \left[\cos(\omega_1 t) - \frac{\gamma}{2\omega_1} \sin(\omega_1 t) \right]. \tag{20}$$

(compare to equation (4)), where

$$\omega_1 \equiv \sqrt{\omega_0^2 - \frac{\gamma^2}{4}} \tag{21}$$

and γ is the friction coefficient. The dynamic structure factor can be expressed analytically now, Fourier transforming equation (3) combined with equation (20), as

$$S(K,\omega) \simeq \mathrm{e}^{-2W} \sum_{j=1}^{\infty} \frac{2^j W^j}{(j-1)!} \left(\frac{\gamma}{(\omega+\omega_1 j)^2 + \gamma^2 j^2/4} + \frac{\gamma}{(\omega-\omega_1 j)^2 + \gamma^2 j^2/4} \right) \tag{22}$$

where $2W \equiv \langle v_{\mathbf{K}}^2 \rangle \frac{\mathbf{K}^2}{\omega_0^2}$ is the Debye–Waller attenuation factor. Equation (22) gives a series of Lorentzians centred at the frequencies $\pm\omega_1$ and their harmonics, with decreasing intensities (typically only the first term of the series, $j = 1$, contributes to the lineshape observed experimentally). The width of the first peak is the friction coefficient γ. Note also that the peak is not centred at the oscillator frequency ω_0 but at ω_1; this is due to the coupling to the bath. Moreover, the **K** dependence enters only through the intensity of the peak by means of the overall attenuation factor, and the T-mode shape is not affected by the wavevector transfer (it is dispersionless) as seen also in QHAS experiments.

Experimentally, the value of the friction coefficient is usually estimated by extrapolation of the width of the T-mode peak to zero temperature, a procedure which is justified by equation (22). When temperature increases, a shift and broadening of the T-mode peak is usually observed, and this can be explained by the anharmonicity of the potential [6]. Recently, we have proposed analytical formulae for the shift and broadening of the T-mode peak, as well as for its anharmonic lineshapes [19], using as a starting point equation (3) and calculating the velocity correlation function $\psi(t)$ by means of a series expansion in the anharmonicity parameter (the next non-zero term in the Taylor expansion of the adiabatic potential around the well minimum). In this way, the experimental shift and broadening can be easily related to the curvature of the adiabatic potential close to the bottom of the potential well. To first order in this curvature, the shift has been shown to be linear with temperature, while to obtain the linear temperature dependence of the broadening one has to go up to second order [19]. The Gaussian approximation is also a very good one for the T-mode peak, opposite to the Q-peak case.

Interestingly, the lineshapes for the T-mode peak can also show a motional narrowing effect similar to the one predicted for the Q-peak in the Gaussian approximation. First we expand the second identity in equation (2) in *moments*, instead of cumulants, and keep to second order (which is equivalent to a second-order Taylor expansion of equation (3) around $\mathbf{K} = 0$). Thus the intermediate scattering function is now proportional to the *position* autocorrelation function. This scattering function can be calculated by assuming a Kubo oscillator model [28] in which the harmonic frequency ω_1 is perturbed by a random frequency including the effect of the anharmonicity. Then one can show [19] that, at long times,

$$I(K,t) \propto \mathrm{Re}\, \mathrm{e}^{\mathrm{i}(\omega_1+\Delta\omega_1)t} \mathrm{e}^{-\gamma t/2} \mathrm{e}^{-\sigma^2 \frac{t^2}{2}} \tag{23}$$

where

$$\sigma = \frac{6|K_4|\langle v_{\mathbf{K}}^2 \rangle}{\omega_1 \omega_0^2} = \frac{\omega_0^2 kT}{2V^{\ddagger}\omega_1 m}. \tag{24}$$

K_4 is the anharmonicity parameter depending on the curvature at the well minimum, and the second equality holds for a 1D cosine potential. When Fourier transforming in time, the first (complex) exponential in equation (23) gives the peak position, with the shift $\Delta\omega_1$ to first order in K_4 [19]. The real exponentials are responsible for the shape and width of the T-mode peak.

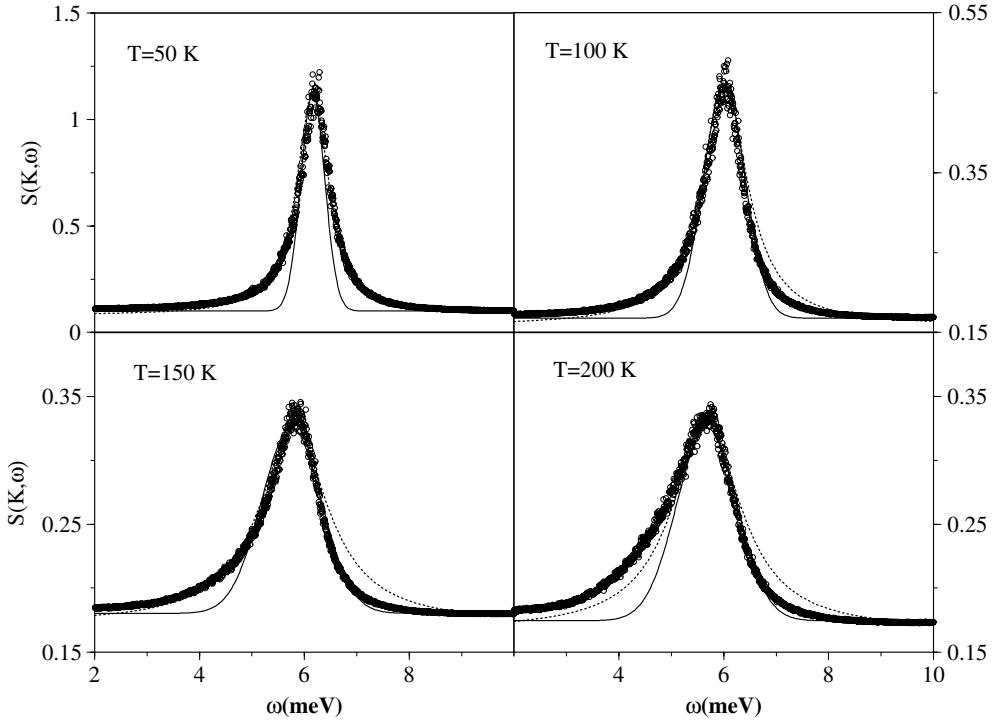

Figure 3. The numerical dynamic structure factor (circles) of the Na/Cu(100) system showing the T-peak lineshape at different temperatures. The solid curves show the Gaussian limit of equation (23) and the dotted ones the Lorentzian limit of this equation.

As seen from equation (23) the motional narrowing is now governed mainly by the parameter σ. If $\sigma \ll 1$ (or $V^{\ddagger}/kT \gg 1$, see equation (24)), the first exponent dominates; the peak has a Lorentzian shape with the FWHM given mainly by γ, as in the harmonic oscillator case. This is easily understood since at high barriers or low temperatures the particle motion is restricted to the vicinity of the potential minimum and the harmonic approximation is a good one. If $\sigma \gg 1$, or $V^{\ddagger}/kT \ll 1$, the Gaussian contribution dominates and the peak has a Gaussian shape with a FWHM mainly given by σ. At intermediate values of σ both contributions have to be taken into account, the central part of the T-mode peak being closer to a Lorentzian while the wings are better approximated to a Gaussian shape.

In figure 3 we show this behaviour for the T-mode peak of the Na/Cu(110) system investigated here. The Fourier transform of the whole intermediate scattering function equation (23), not shown here, reproduces properly the numerical T-mode shape shown with white circles. The dotted curve is the Lorentzian approximation and the solid curve the Gaussian one, taken as limits in equation (23). At higher temperatures the right part of the peak (the one unaffected by overlapping with the Q-peak) is seen to be better approximated by a Gaussian profile, while at low temperatures the Lorentzian is clearly dominant.

4. Mixed diffusion and low vibration lineshapes

A procedure for understanding better some features of the vibrational–diffusional coupling in the adsorbate dynamics consists in assuming a simple model for the velocity autocorrelation

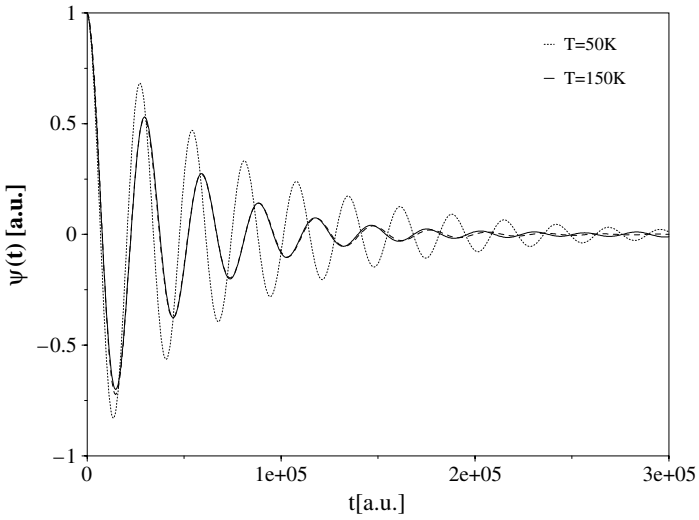

Figure 4. The numerical velocity autocorrelation function for the Na/Cu(100) system at two different temperatures. Dotted curve: $T = 50$ K. Solid curve: $T = 150$ K. The dashed curve is a best fit to the ansatz equation (25) at $T = 150$ K.

function:

$$\psi(t) = \langle u_{\mathbf{K}}^2 \rangle \cos(\omega_2 t + \delta) \mathrm{e}^{-t/\tau_2} \tag{25}$$

where ω_2 gives the T-mode peak position (including the temperature dependent shift) and τ_2 is an overall correlation time. At high temperatures, diffusion is predominant and τ_2 is approximately the diffusion coefficient divided by the scaled temperature kT (see equations (4) and (8)). At low temperatures (for the system studied here, with a diffusion barrier $V^{\ddagger} = 75$ meV, we have $T < 50$ K), jumps among adsorption sites are rare events and the vibrational dynamics is practically the only process. Then $\tau_2^{-1} \sim \gamma/2$; see equation (20). At low temperature, we also have that $\omega_2 \sim \omega_1$, equation (21). The δ phase should be fitted at every temperature.

In figure 4 we show the numerical velocity autocorrelation for the Na/Cu(110) system at two different temperatures: $T = 50$ K (dotted curve) and $T = 150$ K (solid curve). The T-peak shift as well as the faster decay (smaller correlation time) with temperature due to the enhancement of the diffusion process is apparent. The best fit to the analytical ansatz equation (25) at $T = 150$ K is plotted as a dashed curve, showing very good agreement. The parameters taken from the fitting are $\omega_2 = 2.13 \times 10^{-4}$ au and $\tau_2^{-1} = 2.21 \times 10^{-5}$ au. This last value compares well with the friction coefficient $\gamma = 0.1\omega_0 = 2.2 \times 10^{-5}$ au, showing that a decay of the overall correlation function as a free particle model is a good approximation for this temperature.

Now if equation (25) is included in equation (2) (Gaussian approximation) and the integration is carried out analytically, the intermediate scattering function can be written as

$$I(\mathbf{K}, t) = \exp[-\chi^2 f(\omega_2, t)] \mathrm{e}^{-\chi^2 A_1 - \chi^2 A_2 t} \sum_{n,m}^{\infty} \frac{(-1)^n (-1)^m}{n!m!} \chi^{2(n+m)} A_3^n A_4^m \times \mathrm{e}^{-\mathrm{i}(m-n)\delta} \mathrm{e}^{-(m+n)t/\tau_2} \mathrm{e}^{-\mathrm{i}(m-n)\omega_2 t} \tag{26}$$

where χ is given by equation (7) with τ_c replaced by τ_2 (at high temperatures the two values practically agree), and the function $f(\omega_2, t)$ is defined as

$$f(\omega_2, t) = A_1 + A_2 t + A_3 e^{i\delta} e^{-(\tau_2^{-1} - i\omega_2)t} + A_4 e^{-i\delta} e^{-(\tau_2^{-1} + i\omega_2)t} \tag{27}$$

where the coefficients are expressed as

$$A_1 = \frac{\tau_2^{-2}[2\tau_2^{-1}\omega_2 \sin\delta + (\omega_2^2 - \tau_2^{-2})\cos\delta]}{(\tau_2^{-2} + \omega_2^2)^2}, \tag{28}$$

$$A_2 = \frac{\tau_2^{-2}(\tau_2^{-1}\cos\delta - \omega_2 \sin\delta)}{\tau_2^{-2} + \omega_2^2}, \tag{29}$$

$$A_3 = \frac{1}{2\tau_2^2(\tau_2^{-1} - i\omega_2)^2} \tag{30}$$

and

$$A_4 = \frac{1}{2\tau_2^2(\tau_2^{-1} + i\omega_2)^2}. \tag{31}$$

Finally, the dynamic structure factor gives

$$S(\mathbf{K}, \omega) = \frac{e^{-\chi^2 A_1}}{\pi} \sum_{n,m=0}^{\infty} \frac{(-1)^{n+m}\chi^{2(n+m)} A_3^n A_4^m}{n!m!} e^{-i(m-n)\delta} \times \frac{[\chi^2 A_2 + (n+m)\tau_2^{-1}]}{[\omega - (n-m)\omega_2]^2 + [\chi^2 A_2 + (n+m)\tau_2^{-1}]^2}. \tag{32}$$

We have now a double sum over Lorentzian shapes. The Q-peak results from the terms $m = n$ and the T-peaks come from the different combinations of the n and m indices corresponding to the creation and annihilation processes of the T-mode. But again, depending on the χ values, such sums can globally contribute to the two extreme cases, going from a pure Gaussian function to a Lorentzian shape or, even, to intermediate shapes. From equation (32), one can clearly see the contributions of the T-mode to the Q-peak and vice versa. Contrary to what is sometimes stated in the literature, the total lineshape is not a simple sum of two contributions.

In figure 5 we plot the numerical dynamic structure factor for the Na/Cu(100) system at $T = 150$ K (circles) compared with the analytical prediction equation (32) for $\mathbf{K} = 0.11$ Å^{-1}. We have observed that for the range of $\mathbf{K}$ values inside the interval $[0, 0.88]$ Å^{-1}, the Gaussian approximation is valid, that is, equation (32) reproduces very well the lineshapes of the Q- and T-peaks. At larger wavevector transfers (see the inset in figure 5), an appreciable overlapping between the two peaks is apparent and also the Gaussian approximation fails for the quasielastic peak. However, the analytical lineshape remains a very good approximation for the T-mode. This is due to the dispersionless nature of this mode. We remark that the Gaussian approximation for vibrations is accurate not only for all $\mathbf{K}$ values, but also for a wide range of temperatures [19].

At this point of the discussion, we examine to what extent equation (32) could be used as a *working* formula to determine, for the whole first Brillouin zone, what shape (Gaussian-like or Lorentzian-like) displays the Q-peak in a numerical calculation or in an experiment. This is an important issue due to the fact that many times in the deconvolution procedure the shape is assumed in advance. Since equation (32) is obtained with the Gaussian approximation, the corresponding χ value extracted from a fitting procedure will not be in general the same as the nominal one defined by equation (7), once τ_c is replaced by τ_2. In figure 6 we plot the χ value versus the wavevector transfer extracted from the fitting of equation (32) to the numerical simulations at $T = 150$ K. In the inset, we show the quality of the fitting at $\mathbf{K} = 1.23$ Å^{-1} (black

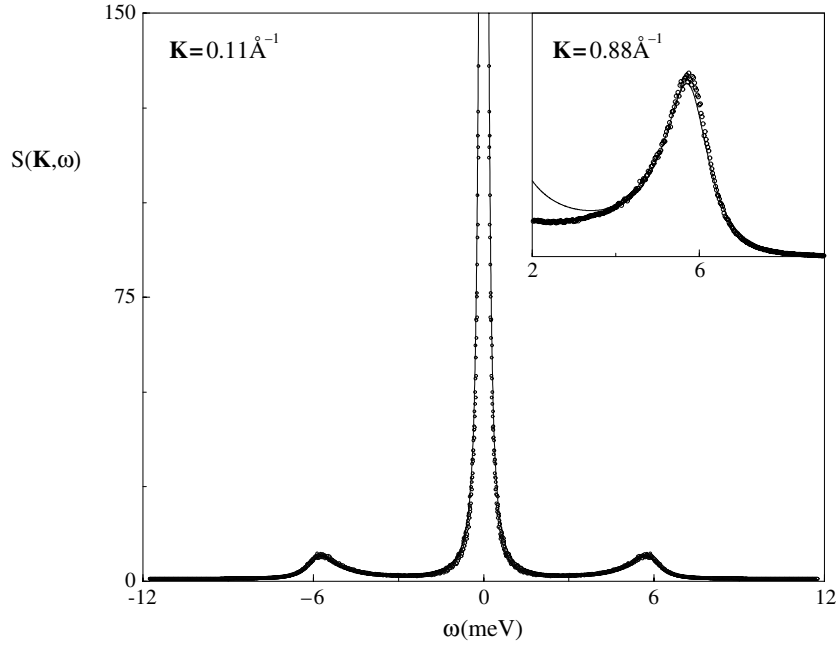

Figure 5. The numerical dynamic structure factor for the Na/Cu(100) system (circles) at $T = 150$ K and $\mathbf{K} = 0.11$ Å^{-1}. Solid line: analytical prediction, (32). In the inset we show an enlargement of the T-peak region at a different value of the wavevector transfer, $\mathbf{K} = 0.88$ Å^{-1}, at the same temperature.

point) once the T-peak is multiplied by a constant factor (in fact, the A_3 and A_4 coefficients in equation (27)). The information we obtain from this analysis is the shape of the Q-peak. At very low and high **K** values the Q-peak approaches a Lorentzian function, and at intermediate values a *mixed* structure is predicted since $\chi \sim 1$. We would like to mention that the effective Lorentzian shape assumed in the deconvolution procedure in [2–4] at high wavevector transfer values is, in our opinion, a weakness of the working method employed there.

5. Inelastic focusing

In recent years, several focusing effects have been reported in inelastic atom–surface scattering. Most such singularities are due to the divergence of the Jacobian (or density of states) of the incident wavevector with respect to the final scattering angle leading to a unified theoretical scheme for their treatments [25]. In particular, a new scattering singularity called the inelastic focusing (IF) effect [24] has also been reported. The IF occurs under special conditions in which the small spread of energies in the incident beam is sharply focused into a very narrow range of final angles. The corresponding mathematical condition is also valid for the *bunching* of the scan curves (curves in the dispersion plane expressing the energy and momentum conservation laws) compatible with the incident parameters (angles and wavevectors) present in the incident beam and around the same value of phonon energy and momentum exchange.

Due to the fact that the origin of most inelastic features can be understood from kinematics, the following in-plane (sagittal) kinematic equations can be taken as the starting point of our theoretical development (square wavevector quantities will be given in energy units in this subsection with $\hbar^2/2m = 1$, m being here the mass of the incident particles): diffraction

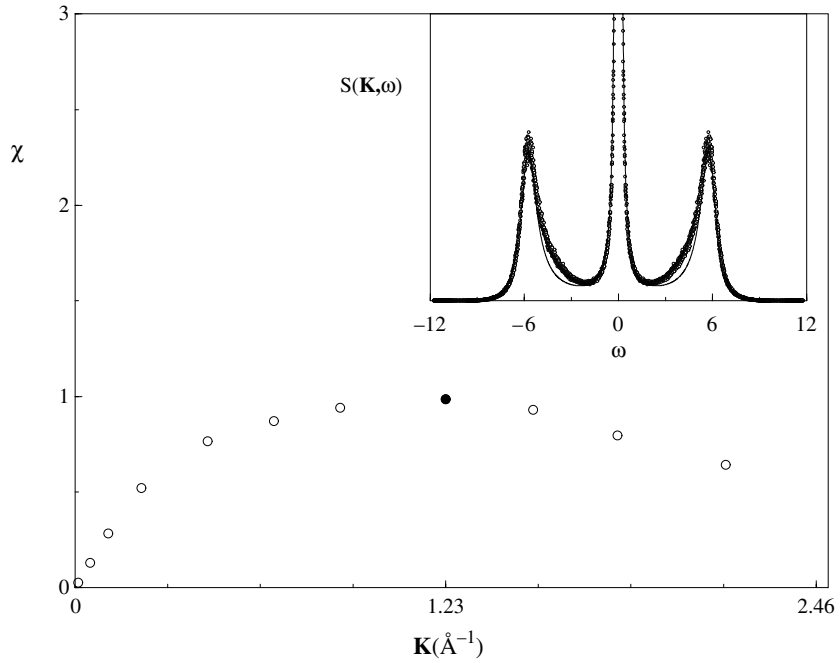

Figure 6. χ in equation (26) as a function of the wavevector transfer **K**, obtained from a procedure of fitting to the numerical lineshapes at $T = 150$ K. In the inset, the quality of the fitting is shown for $\mathbf{K} = 1.23$ Å^{-1} (black point).

condition:

$$\mathbf{K} = \mathbf{k}_\mathrm{f} \sin\theta_\mathrm{f} - \mathbf{k}_\mathrm{i} \sin\theta_\mathrm{i}; \tag{33}$$

energy transfer:

$$\hbar\omega = \mathbf{k}_\mathrm{f}^2 - \mathbf{k}_\mathrm{i}^2; \tag{34}$$

scan curve (SC):

$$\sin\theta_\mathrm{f} = \frac{\mathbf{k}_\mathrm{i} \sin\theta_\mathrm{i} + \mathbf{K}}{\sqrt{\mathbf{k}_\mathrm{i}^2 + \hbar\omega}}, \tag{35}$$

defined in the $(\hbar\omega, \mathbf{K})$ dispersion plane and where $\mathbf{k}_\mathrm{f}$ and $\mathbf{k}_\mathrm{i}$ are the incident and final wavevectors of the incoming particles.

The total in-plane scattering intensity observed experimentally in angular distributions, when a spread of incident energies and angles is present in the incident beam, can be expressed in general in terms of integrals over the incident space and the angular acceptance of the detector of the total differential reflection coefficient, written as [24]

$$\frac{\mathrm{d}R(\mathbf{k}_\mathrm{f}, \mathbf{k}_\mathrm{i})}{\mathrm{d}E_\mathrm{f}\,\mathrm{d}\theta_\mathrm{f}} = \frac{\mathrm{d}R(\mathbf{k}_\mathrm{f}, \mathbf{k}_\mathrm{i})}{\mathrm{d}E_\mathrm{f}\,\mathrm{d}\mathbf{k}_\mathrm{i}} \frac{\mathrm{d}\mathbf{k}_\mathrm{i}}{\mathrm{d}\theta_\mathrm{f}}. \tag{36}$$

The IF singularity occurs when the density of states of $\mathbf{k}_\mathrm{i}$ in the final angular region becomes very large—in other words, when the factor $(\mathrm{d}\theta_\mathrm{f}/\mathrm{d}\mathbf{k}_\mathrm{i})_\mathrm{SC}$ taken along the scan curve is equal to zero. The kinematic condition for such a singularity or bunching of SCs can be finally written as

$$\frac{\mathbf{k}_\mathrm{i}}{\sin\theta_\mathrm{i}} = \frac{\mathbf{k}_\mathrm{f}}{\sin\theta_\mathrm{f}} = \frac{\hbar\omega}{\mathbf{K}}. \tag{37}$$

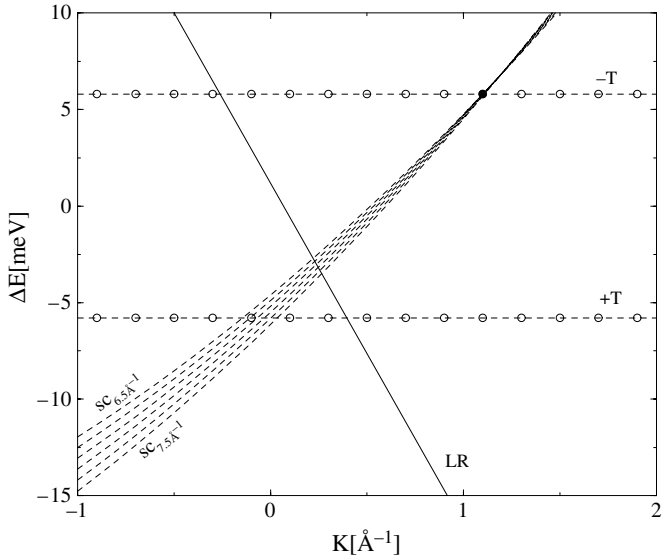

Figure 7. The dispersion plane showing: as a solid line, the longitudinal resonance phonon of the clean substrate Cu(001) along the [100] azimuth; as open circles, the dispersionless T-mode in the creation and annihilation regions; and, as dashed lines, a bunching of scan curves (SC) covering the incident wavevectors between 6.5 and 7.5 Å^{-1} fulfilling the inelastic focusing condition.

Moreover, the IF locus or parametric curve in the dispersion plane depending on $\mathbf{k}_\mathrm{i}$ and keeping the final and incident angles constant, expressed as

$$\begin{aligned} \hbar\omega &= \mathbf{k}_\mathrm{i}^2 \frac{\sin^2\theta_\mathrm{f} - \sin^2\theta_\mathrm{i}}{\sin^2\theta_\mathrm{i}}, \\ \mathbf{K} &= \mathbf{k}_\mathrm{i} \frac{\sin^2\theta_\mathrm{f} - \sin^2\theta_\mathrm{i}}{\sin\theta_\mathrm{i}}, \end{aligned} \tag{38}$$

can be shown to be tangent to the bunching of SCs at the same point. The observation of the IF effect requires that the point of tangency corresponds to some excitation (preferably a surface one). In general, the region of concatenation between the IF locus and the bunching of SCs is quite extended and the focusing condition is fulfilled for a wide range of $\mathbf{k}_\mathrm{i}$ values [24]. Thus, the IF peaks are easy to recognize in angular distributions since they are also placed at *constant angular positions* for those $\mathbf{k}_\mathrm{i}$ values.

As stated above, at low adsorbate concentrations, the corresponding vibrational modes are in a first approximation considered dispersionless. It is always possible to select a set of SCs fulfilling the IF condition for a given $\hbar\omega$ and $\mathbf{K}$ of the dispersionless T-mode. What should be observed is a very sharp peak in time-of-flight spectra converted to an energy transfer scale and therefore possible interference with the quasielastic peak would be drastically reduced—in particular, for higher surface temperatures. Due to the fact that the IF condition can be chosen at will, we could also choose smaller wavevector transfer to sample large distance correlations of adsorbates and control, in a way, the jumping mechanism. Moreover, due to the fact that the entire narrow energy distribution of the incident beam is focused at a single point, the energy resolution of the incident beam does not affect the width of an observable IF feature. As a consequence, as stated for the phonon modes, the natural lifetime of the T-mode will be better estimated eventually without convolution techniques. As an illustration, in figure 7 we display in the dispersion plane the longitudinal resonance (LR) phonon (solid curve) for the clean

Cu(001) substrate along the [100] azimuth, the dotted lines representing the fundamental frequency of the T-mode (5.8 meV) in the creation and annihilation regions, as well as the bunching of scan curves (dashed lines) crossing the T-mode at a given momentum transfer value, $\mathbf{K} = 1.08$ Å^{-1}, and incident angle of 40°, covering an interval of incident wavevectors between 6.5 and 7.5 Å^{-1}. The bunching condition is around the incident wavevector of 7.14 Å^{-1}, after equation (37). It is expected then to have a very sharp T-peak since a bunching of SCs contributes to the lineshape and, if the **K** value is high enough, the diffusion process will not affect the damped vibrational motion. As has been shown elsewhere, any point of the dispersion plane can be easily attained and, therefore, we can control what elementary process we would like to enhance. For example, a triple intersection of curves (T-mode, LR or RW-mode and SCs) can be forced to permit observation of the T-motion assisted by a surface phonon.

6. Conclusions

In this paper we have presented a unified view of diffusional and vibrational motions of adsorbates on surfaces probed in QHAS experiments within a stochastic theoretical framework. We have mainly discussed the Gaussian approximations to the intermediate scattering function for both cases and the lineshapes emerging from theory. A motional narrowing effect can be observed under certain circumstances in the Q-peak as a result of the extension of the theory. For vibration, a motional narrowing effect with increasing temperature (peak profile better approximated by a Gaussian shape) is clearly visible in the Na/Cu(100) system investigated here. We have also proposed a simple analytical model to explain the coupling between diffusion and vibration and showed that, apart from purely diffusive processes, creation and annihilation events whose net energy change is zero also contribute to the shape of the Q-peak. In order to enhance the response of the system and control the optimal conditions to observe diffusion and vibration separately, we have postulated an inelastic focusing effect similar to the one found in other contexts.

Acknowledgments

This work was supported in part by DGCYT (Spain) under contract BFM2001-2179. JLV and RG would like to thank the Ministry of Education and Science (Spain) for a predoctoral grant and a *Ramón y Cajal* Contract, respectively.

References

[1] Ellis J and Toennies J P 1993 *Phys. Rev. Lett.* **70** 2118
[2] Graham A P, Hofmann F, Toennies J P, Chen L Y and Ying S C 1997 *Phys. Rev. Lett.* **78** 3900
[3] Graham A P, Hofmann F, Toennies J P, Chen L Y and Ying S C 1997 *Phys. Rev.* B **56** 10567
[4] Ellis J, Graham A P, Hofmann F and Toennies J P 2001 *Phys. Rev.* B **63** 195408
[5] Jardine A P, Ellis J and Allison W 2002 *J. Phys.: Condens. Matter* **14** 6173
[6] Graham A, Hofmann F and Toennies J P 1996 *J. Chem. Phys.* **104** 5311
[7] Hofmann F and Toennies J P 1996 *Chem. Rev.* **96** 1307
[8] Graham A P and Toennies J P 1998 *Europhys. Lett.* **42** 449
[9] Bertino M, Ellis J, Hofmann F, Toennies J P and Manson J R 1994 *Phys. Rev. Lett.* **73** 605
[10] Van Hove L 1954 *Phys. Rev.* **95** 249
[11] Frenken J W M and Hinch B J 1992 *Helium Atom Scattering from Surfaces* (*Springer Series in Surface Sciences* vol 27) ed E Hulpke (New York: Springer) p 287
[12] Chudley C T and Elliot R J 1961 *Proc. Phys. Soc.* **77** 353
[13] Chen L Y and Ying S C 1993 *Phys. Rev. Lett.* **26** 4361

Chen L Y and Ying S C 1994 *Phys. Rev.* B **49** 13838
Cucchetti A and Ying S C 1999 *Phys. Rev.* B **60** 11110
[14] Guantes R, Vega J L, Miret-Artés S and Pollak E 2003 *J. Chem. Phys.* **119** 2780
[15] Alla-Nissila T and Ying S C 1992 *Prog. Surf. Sci.* **39** 227
[16] Ferrando R, Spadacini R and Tommei G E 1993 *Phys. Rev.* E **48** 2437
[17] Chen L Y, Baldan M R and Ying S C 1996 *Phys. Rev.* B **54** 8856
[18] Pollak E, Bader J, Berne B J and Talkner P 1993 *Phys. Rev. Lett.* **70** 3299
[19] Guantes R, Vega J L, Miret-Artés S and Pollak E 2004 *J. Chem. Phys.* **120** 10768
[20] Vega J L, Guantes R and Miret-Artés S 2002 *J. Phys.: Condens. Matter* **14** 6193
[21] Vega J L, Guantes R, Miret-Artés S and Micha D A 2004 *J. Chem. Phys.* submitted
[22] Van Vleck J H 1948 *Phys. Rev.* **74** 1168
[23] Kubo R 1982 *Fluctuation, Relaxation and Resonance in Magnetic Systems* ed D ter Haar (London: Oliver and Boyd)
[24] Glebov A, Manson J R, Miret-Artés S, Skofronick J G and Toennies J P 1998 *Phys. Rev.* B **57** R9455
[25] Miret-Artés S 1999 *Phys. Rev.* B **60** 1547
[26] Miret-Artés S and Manson J R 2001 *Phys. Rev.* B **63** 121404
[27] Hansen J P and McDonald I R 1986 *Theory of Simple Liquids* (London: Academic)
[28] Kubo R, Toda T and Hashitsume N 1991 *Statistical Physics* vol 2 (Berlin: Springer)
[29] Gardiner C W 1985 *Handbook of Stochastic Methods* (Berlin: Springer)
[30] Ellis J, Graham A P and Toennies J P 1999 *Phys. Rev. Lett.* **82** 5072
[31] Wahnstrom G 1990 *Interactions of Atoms and Molecules with Solid Surfaces* ed V Bortolani, N H March and N P Tosi (New York: Plenum)
[32] Allen M P and Tildesley D J 1987 *Computer Simulations of Liquids* (Oxford: Clarendon)
[33] Pollak E 1996 *Dynamics of Molecules and Chemical Reactions* ed R E Wyatt and J Z H Zhang (New York: Dekker) p 617
[34] Risken H 1989 *The Fokker–Planck Equation* (Berlin: Springer)